Icarus **153**, 285–294 (2001)
doi:10.1006/icar.2001.6701, available online at http://www.idealibrary.com on IDEAL®

Probing Titan's Atmosphere with the 1995 August Stellar Occultation

Philip W. Tracadas,[1] H. B. Hammel,[2,3] J. E. Thomas-Osip, and J. L. Elliot[2,4]

Massachusetts Institute of Technology, 54-410, Department of Earth, Atmospheric, and Planetary Sciences, Cambridge, Massachusetts 02139

and

C. B. Olkin[2]

Lowell Observatory, 1400 West Mars Hill Road, Flagstaff, Arizona 86001

Received February 28, 2000; revised June 21, 2001

On 1995 August 21, Saturn's moon Titan occulted the 13th magnitude star GSC5254-00997. The predawn event was observed at 2.3 μm with the NASA 3.0-m Infrared Telescope Facility. We measured the average atmospheric scale height between latitudes 50°S and 67°S by fitting isothermal models to the immersion portion of the occultation lightcurve. Within the altitude range of 300 to 500 km, we find an isothermal scale height of Titan's sunset atmosphere of 55 ± 9 km. Our derived temperature of 180 ± 30 K is consistent with modeled temperature profiles derived from Voyager 1 IRIS observations (A. Coustenis and B. Bézard 1995, *Icarus* **115, 126–140) and the 28 Sagittarii occultation event (W. B. Hubbard** *et al.* **1993,** *Astron. Astrophys.* **269, 541–563). The atmospheric albedo asymmetry due to low level haze (Caldwell** *et al.* **1992,** *Icarus* **96, 1–9) is inferred from the difference in Titan's center-of-light (determined from precise astrometric measurements of images of Titan and the star before and after the occultation) and the actual center of Titan (determined from the occultation analysis). We find the southern hemisphere to be brighter than the northern hemisphere, a result consistent with Combes** *et al.* **(1997,** *Icarus* **129, 482–497), Gibbard** *et al.* **(1999,** *Icarus* **139, 189–201), and Smith** *et al.* **(1996** *Icarus***, 119, 336–349).**

Key Words: **Titan, atmospheres; structure, occultations.**

I. INTRODUCTION

Titan has long been observed with ground-based telescopes, in the late 1970's with spacecraft (Pioneer 11, Voyagers 1 and 2), and during the past 12 years with radar (Muhleman *et al.* 1995), the Hubble Space Telescope (HST)(Caldwell *et al.* 1992, Smith *et al*. 1996), and stellar occultations (e.g., Hubbard *et al.* 1993). It has been known that Titan has an atmosphere since the discovery of methane in Titan's spectrum (Kuiper 1944), but the size, constituents, and structure of the atmosphere were not well known until Voyager 1's close flyby in 1980. We now know the atmosphere to be dense (about 1.5 bars surface pressure; Tyler *et al.* 1981) and composed mainly of nitrogen gas (Broadfoot *et al*. 1981). Voyager 1 also showed that Titan's surface is shrouded in haze; since then, HST and ground-based telescopes have been used to monitor the changes in this haze's global distribution. The haze prevents visible wavelength observations from detecting the surface, but infrared (Griffith 1993, Lemmon *et al.* 1993, Coustenis *et al.* 1995, Lemmon *et al.* 1995, Smith *et al.* 1996, Combes *et al.* 1997, Gibbard *et al.* 1999) and radar (Muhleman *et al.* 1990, 1995) observations have, respectively, found evidence for large surface features and disproved theories of a global ethane ocean.

The temperature structure and detailed composition of Titan's atmosphere are still under debate. Models by Lellouch *et al.* (1990), Yelle (1991), and Bézard *et al.* (1995) disagree on heating rates and constituents in the upper atmosphere. These models satisfy the sparse Voyager 1 boundary measurements of the atmosphere, but the stratospheric–mesospheric portion of the atmosphere (200–600 km), where Cassini's Huygens probe will experience peak deceleration and heat flux, is not well constrained. The Voyager 1 observations were made during the flyby of Titan in 1980 November (southern autumn). The radio science subsystem (RSS) observations probed the lowest 200 km of Titan's neutral atmosphere using a radio occultation technique (Lindal *et al.* 1983). The infrared interferometer spectrometer (IRIS) observations of the emission in the ν_4 methane band at 7.7 μm were used to infer the temperature between 110 and 260 km (Coustenis and Bézard 1995), and the ultraviolet spectrometer (UVS) observations measured the atmosphere around 1270 km altitude using a solar occultation (Smith *et al.* 1982).

[1] MIT Rm. 54-410; Ph: 617-253-9317; Fax: 617-253-2886. E-mail: tracadas@mit.edu.

[2] Visiting Astronomer at the Infrared Telescope Facility, which is operated by the University of Hawaii under contract to the National Aeronautics and Space Administration.

[3] Now at Space Science Institute, 3100 Marine Street, Suite A353, Boulder, Colorado 80303.

[4] Also at the Department of Physics, MIT, and at Lowell Observatory, Flagstaff, Arizona 86001.

0019-1035/01 $35.00

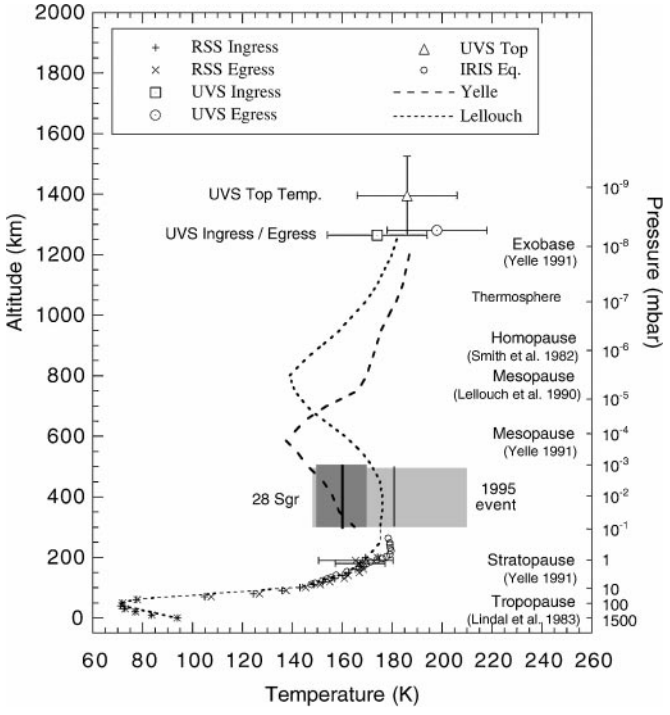

FIG. 1. Titan's temperature profile as a function of altitude and pressure showing all major measurements. The profiles denoted with the symbols + and × are from Voyager 1 radio occultation (RSS) ingress (sunset) and egress (sunrise), respectively (from Lindal *et al.* 1983, and reanalyzed by Lellouch *et al.* 1989). Representative error bars near the 200 km level are 10 and 15°K for the ingress and egress measurements, respectively. The error in both curves drops to 0.5°K at the tropopause and is 0.7°K at the surface. The Voyager 1 UVS observations measured ingress and egress temperatures between 1025 and 1525 km altitude in the thermosphere, but are most sensitive at 1265 km (Smith *et al.* 1982). Temperatures inferred from Voyager 1 IRIS 7.7 μm CH_4 band data from the equatorial regions (Coustenis and Bézard 1995) are depicted with open circles. The shaded regions indicate measurement and errors for each occultation event—the 28 Sgr event (dark shade, Hubbard *et al.* 1993) and our event (light shade). The pressure-to-altitude scale is from Fig. 6 in Strobel *et al.* (1992). For the theoretical temperature profiles of Titan's atmosphere, the dotted line represents the Lellouch *et al.* (1990) model and the dashed line represents the Yelle (1991) model *h*.

Stellar occultations, observed at visual and infrared wavelengths, are able to probe Titan's lower mesosphere directly [see Elliot and Olkin (1996) for a review about using stellar occultations for atmospheric studies]. The occultation of 28 Sagittarii (Sgr) by Titan on 1989 July 3 allowed measurement of the atmospheric temperature (150–170 K), distribution of detached haze, and zonal wind profile as a function of altitude (∼275–500 km) and latitude (Hubbard *et al.* 1993, Sicardy *et al.* 1999). Together with the Voyager observations, these occultation results are the defining measures of the bottom and top of Titan's atmosphere, but they yield an incomplete temperature profile (Fig. 1).

In our analysis, we find that the temperature in the stellar occultation region (lower mesosphere) did not change appreciably from 1989 to 1995. In this paper, we first explain the observations and our method of reduction for our imaged occultation time series. Then, we present the isothermal-model fitting analysis, followed by our results for the scale height, temperature, number density, and pressure in the altitude region to which we are sensitive.

II. OBSERVATIONS

On 1995 August 21, Titan ($V \approx 8.3, K \approx 9.3$) occulted the star GSC5254-00997 (Ansoorian 1993; $V \approx 13.7, K \approx 11.9$). The occultation was observed with the NASA 3.0-m Infrared Telescope Facility (IRTF, Mauna Kea, Hawaii) during the predawn hours while the Saturn system was 32° above the western horizon and the Sun was 8° below the eastern horizon. The center of Titan's shadow passed north of Hawaii's location, indicating that the starlight arriving at the IRTF passed through the southern Titan latitudes (high southern latitudes on western immersion, and equatorial latitudes on eastern emersion as shown in Fig. 2).

The instruments used were the IRTF facility camera NSFCAM with the ("Spencer") 2.3-μm filter and, attached to the optical port, MIT's portable CCD (PCCD) with a 0.89-μm filter. Unfortunately, due to the position of the optical port's focal plane, the PCCD could not be mounted optimally, which resulted in vignetting of the field and poor focus for the optical channel. The resultant lightcurve from the PCCD is of poor quality and hence was not used in this analysis. Observational parameters are summarized in Table I.

The infrared channel's time series lasted over 33 min (9000 frames); the occultation occurred 10 min into this series. Dawn raised the background level above the occultation

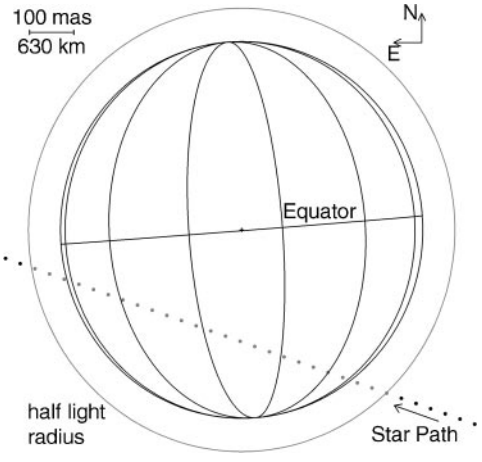

FIG. 2. Titan as viewed from Hawaii during the occultation. The occultation is caused by the relative movement of Titan and the IRTF; the apparent track of the occulted star is plotted here at 10-s intervals. Titan's 5150-km surface diameter subtended 0.82 arcsec at the time of the event; the visible-limb diameter at 2.3 μm is 5260 km or 0.835 arcsec (Toon *et al.* 1992); and the outer circle is the half-light radius (3031 ± 10 km) determined by Sicardy *et al.* (1990) and Hubbard *et al.* (1990). The angular diameter of the star projected to Titan's distance is <20 km. The error in the half-light radius is less than the thickness of its representative line, and the formal error in the star path's impact parameter (±15 km; See Section IV) is the width of the star path dots.

TABLE I
Observational Setup at NASA IRTF

Detector parameters[a]	NSFCAM
Focal plane scale	0.302 ± 0.006 "/pixel
CCD subframe size[b]	48×48 pixels
Sampling interval	224.782 ms[c]
Filter name	"Spencer" 2.3 μm
Filter center	2.275 μm
Filter bandpass (FWHM)	0.172 μm
Data start time[d]	$15^h\ 15^m\ 14.25^s$ UT
Data end time[d]	$15^h\ 48^m\ 57.29^s$ UT

[a] Observers were H. Hammel, J. Elliot, C. Olkin, and C. Kaminski (NASA/IRTF).
[b] The detector used a subframe readout method to minimize readout time.
[c] The actual integration time was 200 ms. The additional ~25 ms is readout and initialization delay time.
[d] The date of the occultation was 1995 08 21.

signal level during the last 3 min of the time series. The rising sun affected the observations only slightly during the time of occultation. At all times during the occultation observations, the signal registered by the detector was well within its linear response region (even during the sunrise portion). Postprocessing of individual frames near the occultation's midpoint showed that Titan's image subtended 5 to 6 pixels (1.5 to 1.8 arcseconds) full-width at half maximum (FWHM). These values can be compared with the diameter of Titan's visible disk of 3 pixels (0.835 arcseconds) at 2.3 μm (Toon *et al.* 1992).

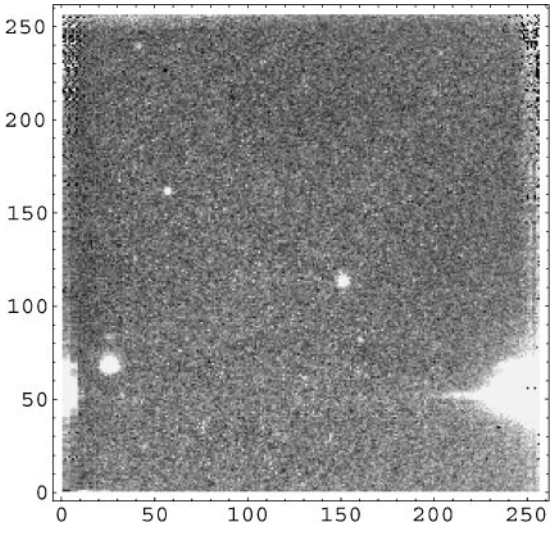

FIG. 3. A full-frame NSFCAM image taken 3.2 h before the occultation (3-s exposure, 2.3-μm filter, dark current and flat field corrected). GSC5254-00997 is at center right (150, 115), Saturn is at the lower right (255, 55) and its reflection is at the far left on nearly the same pixel row (0, 55), and Titan is just above and to the right of this reflection (25, 67). Titan also has an associated bright spot just above it (25, 83) which maintains its relative position and brightness as Titan moves across the field of view. Two neighboring field stars are in the upper left quadrant. North is down and east is to the left in the frame.

NSFCAM was used in "MovieBurst" mode (Leggett and Denault 1996) for the rapid temporal imaging needed for the occultation observations. The initialization and readout times for the detector are not well known (by the standards needed for occultation timing) and are dependent on the chosen subframe size and placement within the full 256×256 pixel detector (Fig. 3). All NSFCAM occultation frames were taken with a 48×48 pixel subframe placed with its northeast corner at row 88 and column 136.

To measure the exact sampling-interval time of NSFCAM in this configuration, a flashing light-emitting diode (LED) was placed in the optical path after the telescope was shut down. The power for the LED was supplied by a TRAK GPS receiver, which generated a precise 100-ms pulse beginning at each second. The same occultation "MovieBurst" mode and subframe were used to record the LED pulsing. Reduction of the LED data yielded a sampling interval between frames of 0.224782 ± 0.000001 sec.

III. REDUCTIONS

The infrared lightcurve was produced from the raw "MovieBurst" images with a marginal analysis technique (Elliot *et al.* 1989) to center a synthetic aperture over the center of light from Titan and the star in each occultation frame. The signals from all pixels within the synthetic aperture were summed to yield the total signal for each time sample. To obtain the optimal lightcurve with maximal signal and minimal background, each frame was measured with synthetic apertures ranging from 10 to 30 pixels square to obtain a family of lightcurves versus aperture size.

Background Correction

Analysis of the background, in individual frames taken near the occultation's midtime, showed that a *quadratus* (the area between two concentric squares) centered on Titan with inner/outer dimensions of 22/30 pixels produced background signal in good agreement with five other background determination techniques (median value, Gaussian fit to the histogram, offset aperture, flux vs. aperture-size curve, and most often occurring value). Hence, our final occultation lightcurve (Fig. 4a) shows signal from a centered 10×10 box (twice the size of Titan's FWHM) with subtraction of background determined from the 22/30 quadratus.

Postoccultation Dip

A postoccultation dip in brightness was observed (Fig. 4a). The correspondence between dip signatures in both the infrared lightcurve and the noisy PCCD curve suggests that individual detector problems are not the cause.

The center of light (determined by marginal analysis) for Titan in absolute frame coordinates showed maximum travel due to tracking drift was limited to less than 10 pixels in either direction. This travel occurred in a generally uniform part of the detector. At or very near the time of the postoccultation dip, the tracking

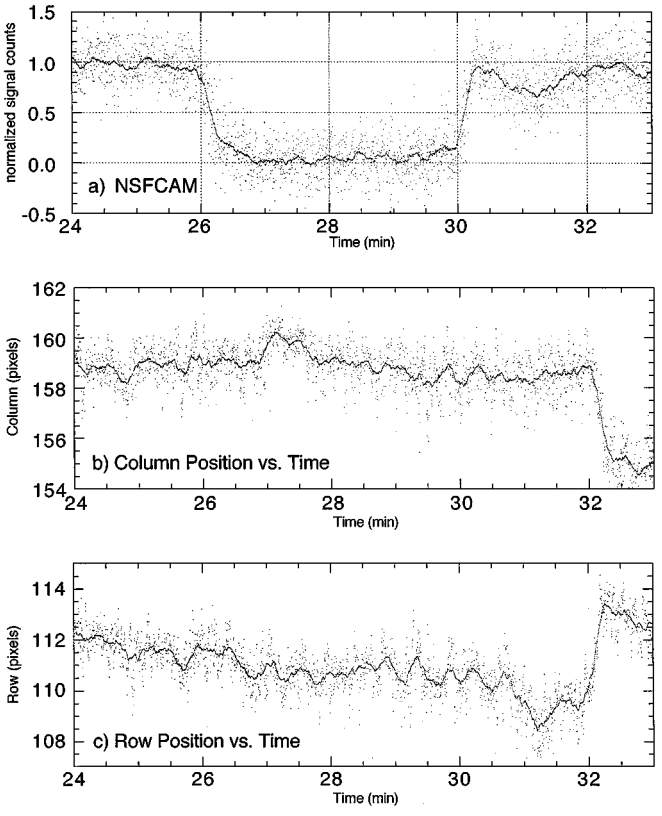

FIG. 4. (a) The occultation lightcurve. This infrared curve (2.3 μm) is unaffected by vignetting in contrast to the simultaneous visual PCCD collected data (not shown), but a dip in the flux immediately after emersion is evident in both curves. Various flat fielding and background subtraction methods have been tried on this segment of the data but the dip is robust. Each datum is a brightness measure from a single occultation frame, and the background has been subtracted (the frames were not flat fielded). (b, c) The travel in column (b) and row (c) of Titan's center-of-light across the NSFCAM detector during the occultation. A significant drifting of the telescope started in the row direction around 30 min 47 s and then the guiding correction reverses the trend in a diagonal direction and ends around 32 min 17 s. In these plots, the dark lines are 50 point (∼11 s) running averages. The time ticks are at 30-s intervals starting at 15:24:00 UT.

drift in the row coordinate increased. Subsequently, a significant guiding correction was applied (apparently after the dip) which moved the center of light a maximum of 6 pixels in less than 30 sec. The increased row drift may have been the cause of the dip since the phase and timing of the movement matches the dip (see Figs. 4b and 4c). Yet, the signal level during the guiding correction does not show any average change in the lightcurve.

No clouds or other atmospheric anomalies were noted during the observations. If we assume the intensity of Titan and the star were affected only during the time of the increased tracking drift and subsequent guiding correction (15:30:47 UT to 15:32:17 UT), then the emersion portion of the lightcurve was not affected until immediately after the preimmersion (unocculted) full level was reached. Unfortunately, the lack of a sustained full level is inadequate for our isothermal model fitting (see the next section) and problematic for making any confident scale height measurements of the emersion region. However, we believe the emersion portion of the lightcurve is still useful for midtime and impact parameter determination.

All of our analyses indicate that the dip is a real occultation event, yet it certainly cannot be readily explained as anything we would believe about Titan and its immediate environment. We leave this as an unexplained feature in the data.

Astrometry

Stare frames (i.e., recorded with all pixels on the NSFCAM detector) were taken before and after the occultation for astrometry and photometry purposes. Since we are limited to observations from a single observatory, the pre- and postevent astrometry measurements are necessary for determining, independently, the closest apparent approach distance between Titan and the star.

Astrometry of Titan and the occultation star were done with both the marginal analysis technique in a "double find" mode and a two-source fitting method that employed a Lorentzian point-spread function. For astrometry when Titan and the star are widely separated, a typical stare frame (Fig. 3) is prepared with background subtraction and flat fielding. Then, in a 50 × 50 aperture around Titan or the star, a marginal analysis is performed. The center value at this step has a large error since the half amplitude points are determined from the difference between the largest row or column sum in the aperture and the background level; the background is determined by a two-pixel ring at the edge of the 50 × 50 aperture. For the "double find," the center of light from this initial marginal analysis is used to center a smaller aperture (10–15 pixels square depending on the object) and the marginal analysis is performed again. This method typically reduces the pixel position error by one or two pixels and corrects completely erroneous initial centers that are offset by up to seven pixels (these cases are due to hot pixels or to the projection of the diagonal alignment of Titan and the star near occultation).

For the occultation frames, in which Titan and the star are merging, both methods were tried. The marginal analysis technique breaks down as Titan and the star come within 6 pixels of each other; the double Lorentzian model (Bosh *et al.* 1992) for the point-spread function is able to give meaningful measurements as the objects come within 2 pixels of each other. The double Lorentzian fits a numerical shape model to the images and has a typical centering error between the two sources of 0.15 pixels.

The relative positions of Titan and the star over the five-hour observing run yield a nearly linear track of motion for Titan across the sky and in time (Fig. 5). Using a second order polynomial fit to the centers from marginal analysis-reduced stare frames and occultation data, our determination of the closest geometric distance of the star's projected approach to the origin of the planet plane (the so-called "impact parameter"; see Fig. 2) is 1350 ± 200 km. With the Lorentzian analysis, the higher quality center positions nearer the occultation allow for good fitting of the ephemeris-predicted star path instead of assuming a polynomial path. The ephemeris star path is useful for its accurate

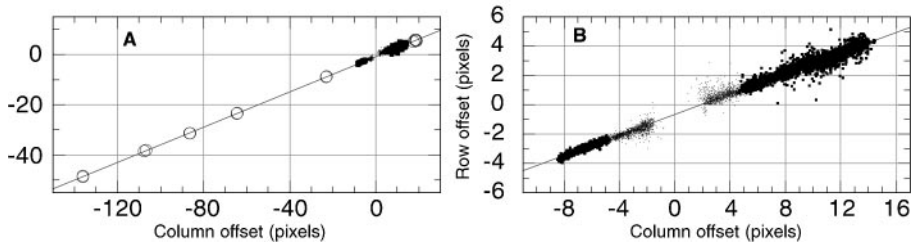

FIG. 5. The motion of Titan relative to GSC5254-00997 over the four hours of observation. The occultation occurs near offset (0, 0) as Titan moved from left (northeast) to right (southwest). We assume the detector maintained constant celestial orientation during the observing night. (A) The open circles are positions from the stare frames; dots and solid squares are measurements from the occultation "movie" frames. (B) In the occultation frames, the absence of offset measurements near (0, 0) is due to the merging of Titan and the star. The solid squares show all offsets measured by the marginal analysis technique; for comparison, the dots show offsets (for the remaining frames) measured by the two-lobed Lorentzian technique (see Section III). In both graphs, the line is both the predicted ephemeris motion and a second order polynomial fit to the observed positions (they are identical at these scales).

relative motions; therefore, the predicted position at mid-occultation gives a better estimate of the center-of-light impact parameter which is 1155 ± 15 km. Comparing this center-of-light impact parameter with the center-of-body impact parameter determined from isothermal model fitting (in Section IV) will allow quantification (as shown in Section V) of the observed hemispheric albedo asymmetry near 2 μm (Combes *et al.* 1997, Gibbard *et al.* 1999).

Photometry

Photometry for both the absolute K magnitude and lightcurve normalization used similar preoccultation, background-subtracted stare frames. UKIRT faint standard star FS32 ($K = 13.664 \pm 0.012$; Casali and Hawarden 1992) was imaged at almost exactly the same air mass and time as Titan and the star. For the facility K filter ($\lambda = 2.21$ μm, FWHM $= 0.39$ μm), flat-field processed images gave Titan's relative K magnitude as ~9.3, compared to the GSC5254-00997 K magnitude of ~11.9. To normalize the NSFCAM lightcurve, the immediate pre- and postoccultation intensity levels of Titan alone (i.e., when the occulted star was not merged or near Titan's image) were averaged to determine the "baseline" light level. The "full" level (i.e., the combined intensity of Titan and the star before or after occultation) was determined from a small segment of the preimmersion portion of the lightcurve.

IV. ISOTHERMAL MODEL FITTING

According to current theoretical models and observations of Titan's atmosphere (Lellouch *et al.* 1990, Yelle 1991, Coustenis and Bézard 1995) and the 28 Sgr occultation inversions (Hubbard *et al.* 1993), the region probed by our stellar occultation (~300–500 km) is roughly isothermal (Fig. 1). This region has a theoretical lapse rate between -0.025 and -0.15 K/km that is not sufficient to affect our lightcurves. A reanalysis of the 28 Sgr lightcurves by Sicardy *et al.* (1999) shows there may be two inversion layers (a sudden increase of T with z) at altitudes of 425 and 455 km in all 28 Sgr profiles. These layers are probably global features of the atmosphere but are not likely to have significant gradients over large enough altitude regions to affect our isothermal models. Hence, to first order, we can assume an isothermal atmosphere.

Using the Elliot and Young (1992, from now on EY92) small planet occultation model, Table II lists model parameters and the resultant best fitted values for the immersion portion of the infrared lightcurve. Inputs to the EY92 model depend solely on the astrometric circumstances of the occultation and the lightcurve; no knowledge of the occulting body's atmospheric constituents is needed (although the atmospheric composition is assumed not to change over the probed altitude range). Since the occultation

TABLE II
Infrared Immersion Lightcurve Model Parameters

Parameter	Fitted or fixed value[a]
Lightcurve full level[b]	1.000 ± 0.005
Lightcurve base level[b]	0.065 ± 0.010
Lightcurve slope[b] (normalized intensity/s)	-0.0004 ± 0.0002
Energy ratio (r_h/scale height)	55.3 ± 8.6
Half-light radius (r_h)	3031 ± 10 km[c]
Mid-time	$15:28:7.3$ UT ± 0.4 s[d]
Impact parameter	1461 ± 15 km[d]
Temperature gradient	0 K/km (isothermal)
Sky-plane velocity	22.012 km/s[e]
Sampling interval	0.224782 s

[a] The included values are for an isothermal, clear (no-haze) fit of the immersion portion of the lightcurve, unless indicated otherwise. Values without errors are fixed. For this fit, the calculated scale height is (r_h/energy ratio) or 55 ± 9 km. Using 1101 data points centered on immersion, this fit's residual variance is 0.03, and the χ^2 is 37 with 1096 degrees of freedom.

[b] The values for these parameters have been transformed to correspond to our normalized lightcurve (see Fig. 5). The original parameter values from our model are 4.025 ± 0.184 s^{-1} for the full level, -0.251 ± 0.063 s^{-1} for the zero flux level (not the base lightcurve level), and -0.0017 ± 0.0010 s^{-1} for the slope.

[c] Value and error from Hubbard *et al.* 1990 and Sicardy *et al.* 1990.

[d] Value from a full fit over the entire lightcurve, excluding the postoccultation dip.

[e] From the DE403 ephemeris (Standish *et al.* 1995). The variation in velocity over the occultation was 0.001 km/s, an error which is negligible compared to our timing uncertainties.

chord passed between 1140 and 1550 km from Titan's center (the impact parameter from derived astrometry; see Section III), no central flash was observed. Thus, the basic model assumptions include near-limb flux only, no extinction, no focusing, and a deep atmosphere (i.e., stellar flux is infinitely bent at smaller radii and not cut off by the satellite's surface).

The Half-Light Radius and Scale Height

The time parameters of the occultation were determined by using the lightcurve's half-intensity times. Determining these times represents the first model attempts and hence, an arbitrary isothermal model was used with the following fixed parameters: sampling interval (see section II), sky-plane velocity, and half-light radius.

The sky-plane velocity was determined through projection of the ephemeris motion of Titan onto the sky plane (motion calculated using the DE403; Standish *et al.* 1995). The calculated velocity of 22.012 km/s is an average over the time length of occultation and has an error of less than 0.001 km/s which is negligible compared to our timing uncertainties. As shown in Section III, Titan's motion in the sky plane was effectively linear in both space and time over the observing time and thus, the sky-plane velocity is assumed constant during the occultation.

We cannot determine the half-light radius with our single chord observation given that the impact parameter determined from astrometry of the pre- and postimaging is related to the center-of-light , which is expected to be offset from the center-of-body due to the hemispheric albedo asymmetry. So we adopt the half-light (or half-intensity) equatorial radius of 3031 ± 10 km from the 28 Sgr occultation (Hubbard *et al.* 1990, Sicardy *et al.* 1990). The half-light radius is wavelength dependent and the longest wavelength of their observations was 0.89 μm; our 2.3-μm observations probe slightly deeper into the atmosphere for a given flux fraction. Available dispersion formulae for nitrogen gas (Washburn 1930, p. 11, Peck and Khanna 1966) are based on experiments using light wavelengths up to 2.0 μm. These dispersion formulae approach an asymptotic value past 3 μm, but are adequate at our observation wavelength to estimate the relative difference in radius probed. The error introduced in the half-light radius by our observation wavelength is only about 0.5% (0.25 km) of a scale height. Our final model results do not change when we use half-light radii over the range 3000–3060 km (three times Sicardy *et al.* (1990) and Hubbard *et al.*'s (1990) errors).

Having determined the sampling interval, the sky-plane velocity, and using the 28 Sgr half-light radius for our preliminary isothermal model, we fit the model to the entire lightcurve from about a minute before immersion half-light (for a good full-level fit) to right after the emersion reaches the immersion full-level but before the postoccultation dip begins. The fitted elapsed time between half-light times is 235.6 ± 0.8 s, with a mid-time at $15:28:7.3$ UT ± 0.4 s. The fitted impact parameter is 1461 ± 15 km. The error in this value is driven by the uncertainty in the half-light radius (10 km). It is important to note, however, that this is based on the assumption that the half-light radius did not change significantly (within its reported errors) between 1989 and 1995.

The impact parameter, taken with the sky-plane velocity direction, also gives a solution for the Titan latitudes probed. The ingress began near 50°S (at the 90% flux level), reached south to 67°S (at the 10% flux level), and finished egress near 5°S (Fig. 2), which are within the latitude coverage of the 28 Sgr event. Our far south ingress point might be affected by atmospheric oblateness. Best fit atmospheric oblateness models to the 28 Sgr occultation central flash by Sicardy *et al.* (1990) and Hubbard *et al.* (1993) measured an oblateness of 0.017 and 0.020, respectively. An oblateness of this magnitude could have affected the half-light radius at our probed latitudes by 32 km.

As stated previously, we varied the half-light radius value of Sicardy *et al.* (1990) and Hubbard *et al.* (1990) over 30 km for ingress and egress without effect on the model results. There is no significant difference between our scale height solution and those determined from the 28 Sgr measurements. Thus our assumption that the half-light radius did not change appreciably between 1989 and 1995 is reasonable and physically plausible. Using the parameters in Table II, we fit another isothermal model to just the ingress portion of the lightcurve to determine the scale height. Our adopted solution (see Table III) has a scale height of 55 ± 9 km, which represents an average value for the region probed by the stellar flux; this region spans from a radius of ~2875 km (~300 km altitude) to a radius of ~3075 km (~500 km altitude).

Sensitivity Testing

The sensitivity of the scale height solution was tested in several ways. The fixed parameters (half-light radius, mid-time, and impact parameter) were each varied from their stated value to the extent of their error and the model refitted. Particular care was taken to understand the correlation between these fixed parameters and the calculated scale height. For example, the mid-time and the impact parameter depend upon each other and greatly affect the scale height value when that dependence is broken (i.e., by fixing these parameters at their extreme error limits without regard to their dependence). In this case, we learn nothing about the scale height error since the model is no longer self-consistent.

The lightcurve's base, full, and slope levels were also studied. By extending the model fit in time before the ingress, the full level changes slightly but does not affect the scale height. The amount of baseline included in the fit affects the scale height because the ultimate baseline value affects the slope determination at half-light. We note that the baseline on the egress portion (Fig. 4a) is higher than for ingress but also has larger variability, possibly due to the onset of the tracking instability and drift. Thus, only the baseline data up to the mid-time were included in our final model. A slope parameter is used for a linear approximation to Titan and the star's signal levels to adjust for the change in air mass during the occultation. The slope is

important because the scale height also depends on the (short time scale) slope at ingress or egress. The fitted slope value given in Table II (in units of normalized flux per second) is significantly different from zero, but the value is small and sensitivity testing about zero slope does not alter our model results significantly. Our ingress model is plotted with the data in Fig. 6.

We note that by fixing the full level and slope of the model, we may fit the egress portion of the lightcurve. Assuming that the egress portion of the lightcurve is unaffected by the postoccultation dip, the scale height value is 37 ± 13 km. It is not statistically different from the ingress value, and the error limits cover the range of scale heights determined by different observatories for the 28 Sgr event (Sicardy *et al.* 1990).

Temperature and Other Model Results

Occultation lightcurves are directly sensitive to the *density* scale height of the atmosphere at and below the half-light radius. If Titan's mesosphere is isothermal and an ideal gas in hydrostatic equilibrium, the density and *pressure* scale heights are equal, and for the ingress (southern sunset) atmosphere they are 55 ± 9 km. This pressure scale height, assuming hydrostatic conditions and that the local gravity at the half-light radius is 97.7 cm s^{-2}, yields a ratio T/μ of 6.5 ± 1.1 K g^{-1}, consistent with the Sicardy *et al.* (1990) value of 6.30 ± 0.75 K g^{-1} and the Hubbard *et al.* (1990) value of 6.54 ± 0.39 K g^{-1}. Following the discussion of Sicardy *et al.* (1990), μ is in the range 27.8–29.4 amu with a preferred value below 27.95 amu, consistent with a nitrogen and methane only atmosphere. The resulting temperature is $6.5 \times 27.8 = 180 \pm 30$ K.

The number density is proportional to the ratio of the refractivities of the atmosphere and the atmospheric gas at standard temperature and pressure. The refractivity of the atmosphere at the half-light level is given to first order by Elliot (1979) and is $2.28 \pm 0.58 \times 10^{-9}$ based on the observed scale height. For the refractivity of the gas, we assume the atmosphere is pure N_2. The refractivity of N_2 at 0°C and 1 atm at an effective wavelength of 2.275 μm is 2.94×10^{-4} (Peck and Khanna 1966). The resultant number density is $2.08 \pm 0.54 \times 10^{14}$ molecules cm^{-3}. Lastly, the pressure can be determined from the ideal gas law. Using our derived temperature and number density, the pressure is 5.2 ± 2.4 μbar at the half-light level of 3031 ± 10 km.

Our single-site observations produced only a single shadow-plane chord, which forces several of our isothermal-model parameters, namely impact parameter or half-light radius, to be either weakly determined with the help of an ephemeris or assumed from the multiple chord solutions of the 28 Sgr occultation. We find there is no significant change in atmospheric scale height (55 ± 9 km) compared to the Hubbard *et al.* (1990) and Sicardy *et al.* (1990) values of 54 ± 6 km. Our temperature (180 ± 30 K) is higher than that found by the 28 Sgr analysis (150–170 K) of the same region, but both measurements are consistent within their error limits and with models of the atmospheric region (Lellouch *et al.* 1990, Yelle 1991, models j and k particularly, Coustenis and Bézard 1995). We summarize our findings in Table III.

TABLE III
Infrared Lightcurve Model Results[a]

Parameter	1995 occultation	1989 occultation
r_h (half-light radius, km)	3031 ± 10[b,c]	3031 ± 10[b,c]
H (scale height at r_h, km)	55 ± 9	56 ± 3[b], 54 ± 6[c]
T_{iso} (K)	180 ± 30	183 ± 11[b], 154–197[c], 150–170[d]
Refractivity	$2.28 \pm 0.58 \times 10^{-9}$	—
Pressure (μbar)	5.2 ± 2.4	5.1 ± 0.3[b], 4.25 ± 0.85[c]
Number density (molecules cm^{-3})	$2.08 \pm 0.54 \times 10^{14}$	$1.95 \pm 0.35 \times 10^{14}$[c]

[a] Clear-atmosphere isothermal small-planet model (EY92), immersion only.
[b] Hubbard *et al.* (1990).
[c] Sicardy *et al.* (1990).
[d] Hubbard *et al.* (1993).

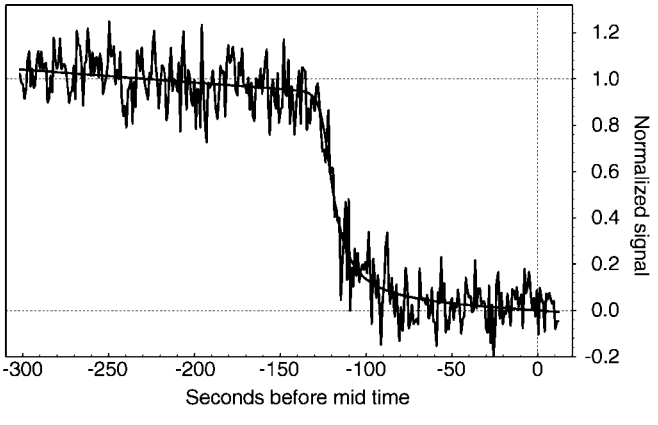

FIG. 6. Adopted isothermal-model fit to the immersion portion of the infrared lightcurve. The model is the smooth, thick line and the data have been smoothed with a four-frame (~1 s) running average. The horizontal axis is seconds before the mid-time (15 : 28 : 7.3 UT).

V. TITAN'S HEMISPHERIC ALBEDO ASYMMETRY

The 28 Sgr data revealed evidence for change in Titan's atmosphere since the Voyager encounters. Hubbard *et al.* (1993) found direct evidence in several south-to-north occultation chords for a denser haze layer above 300 km in Titan's northern (1989's summer) hemisphere compared to southern latitudes (south of 20°S). This hemispheric asymmetry was the *opposite* of that seen in the Voyager 2 high phase-angle limb image data (Rages and Pollack 1983), which are also sensitive to the density of the atmosphere's detached haze (between 300 and 350 km altitude).

Other Voyager 1 image data, taken at moderate phase angles, showed that the haze layer that shrouds Titan at visible wavelengths had a hemispheric albedo asymmetry, with the southern hemisphere being brighter than the northern (Smith *et al.* 1981, Sromovsky *et al.* 1981). According to Toon *et al.*

(1992), Titan's atmospheric circulation can explicitly reverse in response to northern solar heating. This predicted change in Titan's atmospheric circulation—hinted at in the 1989 28 Sgr haze extinction observations—was confirmed directly by Hubble Space Telescope (HST) observations of Titan's atmosphere taken in August 1990 (Caldwell *et al.* 1992). In passbands comparable to those of Voyager 1 (i.e., 0.439 and 0.547 μm), deconvolved HST images showed the north to be brighter than the southern hemisphere. Importantly, simultaneous HST images at 0.889 μm showed the opposite orientation (bright southern hemisphere), a characteristic reversal which Toon *et al.*'s (1992) model had predicted for wavelengths longer than 0.6 μm. In 1994, further HST imaging showed that the asymmetry of 1990 (at wavelengths longer than 0.6 μm) was still in effect (Smith *et al.* 1996).

Additionally, fourteen HST images were taken of Titan in September and October of 1995, just two months (or four revolutions) after our occultation and over a year after the equinox (Caldwell *et al.* 1996). The hemispheric asymmetry was evident in the October 1994 calibrated images by using a simple contrast stretch. The 180° change in the asymmetry orientation shortward and longward of 0.6 μm was also evident. Furthermore, ground-based observations in 1994 and 1995 near 2 μm also show this hemispheric asymmetry. Combes *et al.* (1997) report a 20–30% brightness contrast between the brighter southern hemisphere and the northern one in their K2 filter at 2.2 μm and Gibbard *et al.* (1999) also show a brighter southern hemisphere in the K' filter at 2.1 μm.

In order to quantify the hemispheric asymmetry, we constructed synthetic Titans with a range of simulated north to south albedo ratios and fit them with a single Lorentzian function to determine the offset between the center-of-light and the center-of-body. The equator of Titan is seen almost side-on (subearth latitude is about a quarter of a degree) and hence both hemispheres have roughly equal projected areas. The synthetic model, incorporating limb darkening and a telescope seeing blur while assuming a uniform albedo for each hemisphere, yields an offset of the center-of-light due south along the Titan subearth meridian from the center-of-figure as shown in the bottom panel in Fig. 7. The center-of-body impact parameter and the resultant half-light radius can then be determined geometrically and are also plotted in Fig. 7. If we make the assumption that the half-light radius has not changed substantially since the 1989 occultation of 28 Sgr, as was done in the previous section, then this would imply a north–south albedo ratio near 0.6 and thus a contrast difference of 40%, which is slightly higher than that found by Combes *et al.* (1997) at 2.2 μm. If the offset as calculated from the center-of-body impact parameter determined from the 28 Sgr half-light radius, and the center-of-light impact parameter as calculated from our astrometry, is not due to the albedo asymmetry but rather reflects a real change in the half-light radius, then this would imply that the half-light radius had decreased from 3031 in 1989 to 2890 km in 1995. This is a physically unrealistic change requiring a reduction in the surface pressure by a factor of 8 for the same temperature structure.

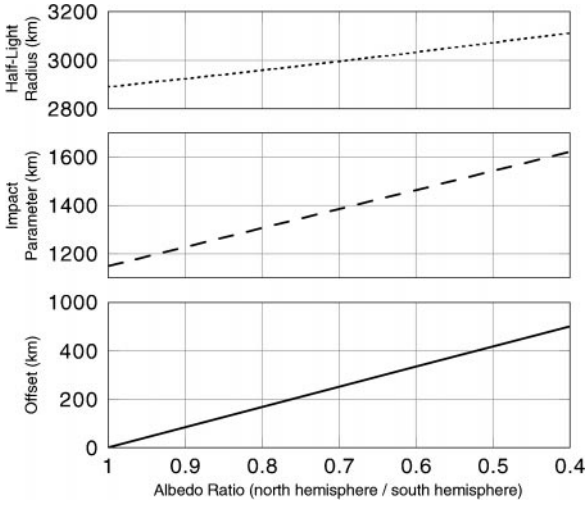

FIG. 7. The effect of varying the hemispheric albedo asymmetry versus center-of-light/center-of-body offset, impact parameter, and half-light radius. For these functions, a synthetic Titan was constructed with the same pixel scale as our observations and a fixed southern hemisphere albedo of 1 (see Section III). The solid line shows the offset of Titan's center-of-light from its center-of-body (the formal error of the Lorentzian fit at this pixel scale along with the error from varying Titan's subpixel center is about ±100 km); the impact parameter (dashed line) is computed assuming the offset is due south along the Titan subearth meridian; the half-light radius (dotted line) is calculated from the occultation length and the resultant impact parameter.

The event analyzed here took place shortly past the equinox as the northern hemisphere entered its "winter" and tracked an unobserved phase of Titan's annual cycle at these altitudes (Fig. 8).

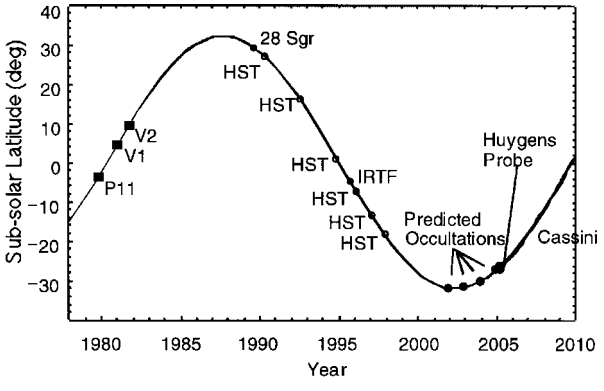

FIG. 8. Titan's seasonal aspect as a function of year. Also indicated are dates of spacecraft encounters (Pioneer 11, Voyagers 1 and 2); the widely observed 28 Sgr occultation (e.g., Hubbard *et al.* 1993); HST imaging in 1990 (Caldwell *et al.* 1992), 1992 (Smith and Lemmon 1993), 1994 (Smith *et al.* 1996), 1995 (Caldwell *et al.* 1996, Karkoschka and Lorenz 1997), 1996 (Young 1996), and 1997 (Lemmon 1997, Smith 1997); this paper's occultation (21 August 1995); occultations predicted in the near future (Amanda S. Bosh and Larry H. Wasserman, personal communication, 2000), and the expected span of the Cassini mission along with the Huygens probe entry date. Adapted from Hubbard *et al.* (1993).

If the haze asymmetry flip, which occurred sometime between Voyager observations in 1980 (near Titan equinox as the northern hemisphere entered its "summer") and the 1989 occultation, is a product of a lagged atmospheric seasonal response to solar heating, then it is expected that another asymmetry reversal would take place before the Cassini encounter (beginning just after the northern summer solstice). Further monitoring of Titan via multiple chord occultation observations will help determine the time of this reversal as well as characterize the nature of the variation at the time of reversal.

VI. SUMMARY

Our single-chord observations of the Titan occultation of 1995 August 21 yield a scale height and temperature consistent with the 1989 occultation measurements. Assuming an atmosphere made totally of nitrogen in hydrostatic equilibrium, we find that the temperature in the isothermal region between $\sim$300 and 500 km is 180 ± 30 K, and the average scale height in the region is 55 ± 9 km. A novel application of occultation observation analysis has been made to demonstrate a method for inferring the albedo asymmetry ratio by examining the difference between the center-of-light impact parameter (as determined by precise astrometric measurements of the pre- and postevent images) and the center-of-body impact parameter (as determined from the analysis of the occultation).

The Cassini mission and its Huygens probe will arrive at the Saturn system in 2004, possibly during a stable period between seasonal change events (the mission will arrive soon after the beginning of northern winter and is planned to stop before the equinox). Continued observations of Titan to document the nature of this changing atmosphere may significantly enhance mission planning. The method for determining the hemispheric albedo ratio presented here demonstrates the value of continued multiple chord occultation observations of Titan (so that the center-of-body can be established simultaneously with the center-of-light determination). Such data, in conjunction with HST and ground-based imaging in the immediate future, may reveal the timing of the albedo reversal at different haze levels, and hence the length and character of the solar phase lag.

ACKNOWLEDGMENTS

We are grateful to the IRTF staff, who helped install our instrument and operated the telescope for our observations. We thank Athena Coustenis and Bill Hubbard for their reviews that helped to significantly improve this paper. Partial support for this work was provided by NSF Grants AST-9322115 and AST-0073447.

REFERENCES

Ansoorian, C. 1993. *A Determination of Titan Stellar Occultation Candidates for the Time Period January 1993 through December 1999.* S.B. thesis, Massachusetts Institute of Technology, Cambridge.

Bezard, B., A. Coustenis, and C. P. McKay 1995. Titan's stratospheric temperature asymmetry: A radiative origin? *Icarus* **113**, 267–276.

Bosh, A. S., L. A. Young, J. L. Elliot, H. B. Hammel, and R. L. Baron 1992. Photometric variability of Charon at 2.2 μm. *Icarus* **95**, 319–324.

Broadfoot, A. L., B. R. Sandel, D. E. Shemansky, J. B. Holberg, G. R. Smith, D. F. Strobel, J. C. McConnell, S. Kumar, D. M. Hunten, S. K. Atreya, T. M. Donahue, H. W. Moos, J. L. Bertaux, J. E. Blamont, R. B. Pomphrey, and S. Linick 1981. Extreme ultraviolet observations from Voyager 1 encounter with Saturn. *Science* **212**, 206–211.

Caldwell, J., C. C. Cunningham, D. Anthony, H. P. White, E. J. Groth, H. Hasan, K. Noll, P. H. Smith, M. G. Tomasko, and H. A. Weaver 1992. Titan: Evidence for seasonal change—a comparison of Hubble Space Telescope and Voyager images. *Icarus* **96**, 1–9.

Caldwell, J., N. Wu, P. H. Smith, R. D. Lorenz, and M. T. Lemmon 1996. Hubble Space Telescope imaging of Titan in 1995. *Bull. Am. Astron. Soc.* **28**, 2015.

Casali, M. M., and T. G. Hawarden 1992. UKIRT provisional faint standards. *JCMT–UKIRT Newsletter* **3**, 33.

Combes, M., L. Vapillon, E. Gendron, A. Coustenis, O. Lai, R. Wittemberg, and R. Sirdey 1997. Spatially resolved images of Titan by means of adaptive optics. *Icarus* **129**, 482–497.

Coustenis, A., E. Lellouch, J.-P. Maillard, and C. P. McKay 1995. Titan's surface: Composition and variability from the near-infrared albedo. *Icarus* **118**, 87–104.

Coustenis, A., and B. Bézard 1995. Titan's atmosphere from Voyager infrared observations. IV. Latitude variations of temperature and composition. *Icarus*. **115**, 126–140.

Elliot, J. L. 1979. Stellar occultation studies of the Solar System. *Annu. Rev. Astron. Astrophys.* **17**, 445–475.

Elliot, J. L., E. W. Dunham, R. L. Baron, A. W. Watts, S. P. Kruse, W. R. Rose, and C. M. Gillespie 1989. Image quality of the Kuiper Airborne Observatory. I. Results of the first flight series. *Publ. Astron. Soc. Pacific*. **101**, 737–764.

Elliot, J. L., and C. B. Olkin 1996. Probing planetary atmospheres with stellar occultations. In *Annual Review of Earth and Planetary Sciences* (G. W. Wetherill, Ed.), pp. 89–123. Annual Reviews, Palo Alto, CA.

Elliot, J. L., and L. A. Young 1992. Analysis of stellar occultation data for planetary atmospheres. I. Model fitting, with application to Pluto. *Astron. J.* **103**, 991–1015.

Gibbard, S. E., B. Macintosh, D. Gavel, C. E. Max, I. de Pater, A. M. Ghez, E. F. Young, and C. P. McKay 1999. Titan: High-resolution speckle images from the Keck telescope. *Icarus* **139**, 189–201.

Griffith, C. A. 1993. Evidence for surface heterogeneity of Titan. *Nature* **364**, 511–513.

Hubbard, W. B., D. M. Hunten, H. J. Reitsema, N. Brosch, Y. Nevo, E. Carreira, F. Rossi, and L. H. Wasserman 1990. Results for Titan's atmosphere from its occultation of 28 Sagittarii. *Nature* **343**, 353–355.

Hubbard, W. B., B. Sicardy, R. Miles, A. J. Hollis, R. W. Forrest, I. K. M. Nicolson, G. Appleby, W. Beisker, C. Bittner, H.-J. Bode, M. Bruns, H. Denzau, M. Nezel, E. Riedel, H. Struckmann, J. E. Arlot, F. Roques, F. Sévre, W. Thuillot, M. Hoffman, E. H. Geyer, C. Buil, F. Colas, J. Lecacheux, A. Klotz, E. Thouvenot, J. L. Vidal, E. Carreria, F. Rossi, C. Blanco, S. Cristaldi, Y. Nevo, H. J. Reitsema, N. Brosch, K. Cernis, K. Zdanavicius, L. H. Wasserman, D. M. Hunten, D. Gautier, E. Lellouch, R. V. Yelle, B. Rizk, F. M. Flasar, C. C. Porco, D. Toublanc, and G. Corugedo 1993. The occultation of 28 Sgr by Titan. *Astron. Astrophys.* **269**, 541–563.

Karkoschka, E., and R. D. Lorenz 1997. Latitudinal variation of aerosol sizes inferred from Titan's shadow. *Icarus* **125**, 369–379.

Kuiper, G. P. 1944. Titan: A satellite with an atmosphere. *Astrophys. J.* **100**, 378–383.

Leggett, S., and T. Denault 1996. *NSFCAM* 256×256 *InSb Infrared Array Camera User's Guide.* NASA Infrared Telescope Facility http://irtf.ifa.hawaii.edu/Facility/nsfcam/nsfcam.html.

Lellouch, E., A. Coustenis, D. Gautier, F. Raulin, N. Dubouloz, and C. Frère 1989. Titan's atmosphere and hypothesized ocean: A reanalysis of the Voyager 1 radio-occultation and IRIS 7.7 μm data. *Icarus.* **79**, 328–349.

Lellouch, E., D. M. Hunten, G. Kockarts, and A. Coustenis 1990. Titan's thermosphere profile. *Icarus* **83**, 308–324.

Lemmon, M. T., E. Karkoschka, and M. G. Tomasko 1993. Titan's rotation: Surface feature observed. *Icarus* **103**, 329–332.

Lemmon, M. T., E. Karkoschka, and M. G. Tomasko 1995. Titan's rotational lightcurve. *Icarus* **113**, 27–38.

Lemmon, M. T. 1997. Spatially resoved multispectral investigation of Titan's troposphere and stratosphere. Space Telescope Science Institute Web Archive, http://archive.stsci.edu, proposal 7321, cycle 7.

Lindal, G. F., G. E. Wood, H. B. Hotz, D. N. Sweetnam, V. R. Eshleman, and G. L. Tyler 1983. The atmosphere of Titan: An analysis of the Voyager 1 radio occultation measurements. *Icarus* **53**, 348–363.

Muhleman, D. O., A. W. Grossman, B. J. Butler, and M. A. Slade 1990. Radar reflectivity of Titan. *Science* **248**, 975–980.

Muhleman, D. O., A. W. Grossman, and B. J. Butler 1995. Radar investigations of Mars, Mercury, and Titan. *Annu. Rev. Earth Planet. Sci.* **23**, 337–374.

Peck, E. R., and B. N. Khanna 1966. Dispersion of nitrogen. *J. Opt. Soc. Am.* **56**, 1059–1063.

Rages, K., and J. B. Pollack 1983. Vertical distribution of scattering hazes in Titan's upper atmosphere. *Icarus* **55**, 50–62.

Sicardy, B., A. Brahic, C. Ferrari, D. Gautier, J. Lecacheux, E. Lellouch, F. Roques, J. E. Arlot, F. Colas, W. Thuillot, F. Sevre, J. L. Vidal, C. Blanco, S. Cristaldi, C. Buil, A. Klotz, and E. Thouvenot 1990. Probing Titan's atmosphere by stellar occultation. *Nature* **343**, 350–353.

Sicardy, B., F. Ferri, F. Roques, J. Lecacheux, S. Pau, N. Brosch, Y. Nevo, W. B. Hubbard, H. J. Reitsema, C. Blanco, E. Carreira, W. Beisker, C. Bittner, H.-J. Bode, M. Bruns, H. Denzau, M. Nezel, E. Riedel, H. Struckmann, G. Appleby, R. W. Forrest, I. K. M. Nicolson, A. J. Hollis, and R. Miles 1999. The structure of Titan's stratosphere from the 28 Sgr occultation. *Icarus* **142**, 357–390.

Smith, B. A., L. Soderblom, R. Beebe, J. Boyce, G. Briggs, A. Bunker, S. A. Collins, C. J. Hansen, T. V. Johnson, J. L. Mitchell, R. J. Terrile, M. Carr, A. F. Cook, II, J. Cuzzi, J. B. Pollack, G. E. Danielson, A. Ingersoll, M. E. Davies, G. E. Hunt, H. Masursky, E. Shoemaker, D. Morrison, T. Owen, C. Sagan, J. Veverka, R. Strom, and V. E. Suomi 1981. Encounter with Saturn: Voyager 1 imaging science results. *Science* **212**, 163–191.

Smith, G. R., D. F. Strobel, A. L. Broadfoot, B. R. Sandel, D. E. Shemansky, and J. B. Holberg 1982. Titan's upper atmosphere: Composition and temperature from the EUV solar occultation results. *J. Geophys. Res.* **87**, 1351–1359.

Smith, P. H., M. T. Lemmon, R. D. Lorenz, L. A. Sromovsky, J. J. Caldwell, and M. D. Allison 1996. Titan's surface, revealed by HST imaging. *Icarus.* **119**, 336–349.

Smith, B. A. 1997. Surface and atmospheric features on Titan. Space Telescope Science Institute Web Archive, http://archive.stsci.edu, proposal 7180, cycle 7.

Smith, P. H., and M. T. Lemmon 1993. HST images of Titan. *Bull. Am. Astron. Soc.* **26,** 1105.

Sromovsky, L. A., V. E. Suomi, J. B. Pollack, R. J. Krauss, S. S. Limaye, T. Owen, H. E. Revercomb, and C. Sagan 1981. Implications of Titan's north–south brightness asymmetry. *Nature* **292**, 698–702.

Standish, E. M., X. X. Newhall, J. G. Williams, and W. M. Folkner 1995. *JPL Planetary and Lunar Ephemerides, DE403/LE403.* Jet Propulsion Laboratory, Pasadena.

Strobel, D. F., M. E. Summers, and X. Zhu 1992. Titan's upper atmosphere: Structure and ultraviolet emissions. *Icarus* **100**, 512–526.

Toon, O. B., C. P. McKay, C. A. Griffith, and R. P. Turco 1992. A physical model of Titan's aerosols. *Icarus* **95**, 24–54.

Tyler, G. L., V. R. Eshleman, J. D. Anderson, G. S. Levy, G. F. Lindal, G. E. Wood, and T. A. Croft 1981. Radio science investigations of the Saturn system with Voyager 1: Preliminary results. *Science* **212**, 201–206.

Washburn, E. W. 1930. *International Critical Tables of Numerical Data—Physics, Chemistry, and Technology.* McGraw–Hill, New York.

Yelle, R. V. 1991. Non-LTE models of Titan's upper atmosphere. *Astrophys. J.* **383**, 380–400.

Young, E. F. 1996. Spatially resolved mapping of Titan's atmosphere at several interesting wavelengths. Space Telescope Science Institute Web Archive, http://archive.stsci.edu, proposal 6733, cycle 6.